DEVELOPMENT OF A RECURRENT NEURAL NETWORK BASED ESTIMATION ALGORITHMS FOR ANKLE POWER BY USING SURFACE EMG.

by

Alper Atal

B.S., in Industrial Product Design, Istanbul Technical University, 2019

Submitted to the Institute of Biomedical Engineering
in partial fulfillment of the requirements
for the degree of
Master of Science
in
Biomedical Engineering

Boğaziçi University
2022

ACKNOWLEDGMENTS

I would like to thank to my supervisor, Prof. Dr. Can Yucesoy for his enlightening guidance through my master studies. I feel honoured to study under him. I am grateful for his understanding and concern. I would also like to express my appreciation to the committee for reviewing and recommendations.

I would like to thank to my friends Tarik Turksoy, Engin Kaya and Onur Rodop for their support on the understanding of MatLAB. I would like to thank to my wife Ezgi Atal for her love and unending support through all.

ACADEMIC ETHICS AND INTEGRITY STATEMENT

hereby certify that I am aware of the Academic Ethics and Integrity Policy issued by the Council of Higher Education (YÖK) and I fully acknowledge all the consequences due to its violation by plagiarism or any other way.

Name :

Signature:

Date:

ABSTRACT

DEVELOPMENT OF A RECURRENT NEURAL NETWORK BASED ESTIMATION ALGORITHMS FOR ANKLE POWER BY USING SURFACE EMG.

Estimation of ankle power can be used in identification of gait abnormalities and establishing timings of net power generation in powered prosthetic devices. Current inverse dynamics calculations of ankle power rely on gait analysis data collected in specialized, expensive laboratories, which limits its applicability and accessibility for prosthetic device users. The aim of this study is to develop a Recurrent Neural Network system to estimate ankle power during level walking by using only surface electromyography (sEMG) as algorithm inputs. For this purpose, an open access data set which includes 50 participants with 25 males and 25 females aged between 6 to 72. In the dataset there are sEMG data from upper leg muscles: Biceps Femoris (BF), Gastrocnemius Medialis (GM), Gluteus Maximum (GMax), Rectus Femoris (RF), Vastus Medialis (VM) and lower body muscles; Peroneus Longus (PL), Soleus (SO), Tibialis Anterior (TA). Algorithms for combinations of all these muscles have been developed. A correlation coefficient of 0.90 between the actual (result of gait analysis) and predicted ankle power is considered to perform successfully. 25 muscle combinations yielded successful correlations with 1 set of 1 muscle, 3 sets of 2 muscles, 5 sets of 3 muscles, 9 sets of 4 muscles, 5 sets of 5 muscles, 1 set of 6 muscles, 1 set of 7 muscles. Note that, all successful muscle groups include either PL or GM muscle. Our findings suggest that our system can be used in powered prosthetics control and detection of gait abnormalities.

Keywords: Ankle Power, Electromyography, Walking, Artificial Neural Networks.

ÖZET

YÜZEYSEL ELEKTROMİYOGRAFİ VERİSİ İLE YÜRUYÜŞ ESNASINDA AYAK BİLEĞİNDEKİ GÜÇÜ TAHMİN EDEN YİNELEMLİ SİNİR AĞI ÜRETİMİ.

Ayak bileği gücünün tahmini, yürüyüş anormalliklerinin tanımlanmasında ve elektrikli protez cihazlarda net güç üretiminin zamanlamasının belirlenmesinde kullanılabilir. Ayak bileği gücünün mevcut ters dinamik hesaplamaları, prostetik cihaz kullanıcıları için uygulanabilirliğini ve erişilebilirliğini sınırlayan, uzmanlaşmış, pahalı laboratuvarlarda toplanan yürüyüş analizi verilerine dayanmaktadır. Bu çalışmanın amacı, algoritma girdileri olarak sadece yüzey elektromiyografisini kullanarak düz yürüme sırasında ayak bileği gücünü tahmin etmek için bir Tekrarlayan Sinir Ağı sistemi geliştirmektir. Bu amaçla, yaşları 6 ile 72 arasında değişen 25 erkek ve 25 kadından oluşan 50 katılımcının yer aldığı açık erişimli bir veri seti. Veri setinde üst bacak kaslarına ait sEMG verileri bulunmaktadır: Biceps Femoris (BF), Gastrocnemius Medialis (GM), Gluteus Maximum (GMax), Rectus Femoris (RF), Vastus Medialis (VM) ve alt vücut kasları; Peroneus Longus (PL), Soleus (SO), Tibialis Anterior (TA). Tüm bu kasların kombinasyonları için algoritmalar geliştirilmiştir. Gerçek (yürüyüş analizinin sonucu) ve tahmin edilen ayak bileği gücü arasında 0.90'lık bir korelasyon katsayısı bu çalışma için başarılı bir performans olarak kabul edilmiştir. 25 kas kombinasyonunda başarılı sonuç alindi. Tüm başarılı kas gruplarının ya PL ya da GM kasını gözlemlendi. Bulgularımız, sistemimizin güçlü protez kontrolünde ve yürüyüş anormalliklerinin tespitinde kullanılabileceğini düşündürmektedir.

Anahtar Sözcükler: Yapay Zeka, Bilek, Güc, Enerji, Yürüyüs, Elektromiyografi.

TABLE OF CONTENTS

LIST OF FIGURES

LIST OF TABLES

LIST OF ABBREVIATIONS

EMG	Electromyography
sEMG	Surface Electromyography
VM	Vastus Medialis
GMax	Gluteus Maximum
GM	Gastrocnemius Medialis
BF	Biceps Femoris
RF	Rectus Femoris
TA	Tibialis Anterior
SO	Soleus
PL	Peroneus Longus
NN	Neural Network
ANN	Artificial Neural Network
RNN	Visual Evoked Potential
LSTM	Long Short-Term Memory
RMSE	Root Mean Square Error
MAF	Moving Average Filtering
ML	Machine Learning
MUAP	Motor Unit Action Potential
MUAPt	Motor Unit Action Potential Train

1. INTRODUCTION

Walking is at the centre of the human locomotion, from long distance strides to small pacing inside house. Since the time of the Aristotle humankind tried to understand the human walking. In the enlightenment wind of the renaissance, scientist try to establish quantitative methods to understand human locomotion. In the renaissance era the idea of estimating the values of human walking planted by Girolamo Cardan. Giovanni Alfonso Borelli made the first gait analysis in the 17th century. Figure 1.1 show one part of the Borelli's human motion studies. With his initial experiments he gathered information about mechanics of the muscles and the quantification of forces in the muscles and the tendons. In the 19th century gait visual recording have been implemented to the gait analysis. In the following years gait analysis have been integrated with the 3-dimensional measurement methods. Usage of Geisser tube strapped body suit in a dark room is the first iteration of the 3D visual markers. The suit is shown in the Figure 1.1. In later research force plates, which are used to calculate ground reaction forces added in the standard procedure of the gait analysis. In the years between 1945 and 1960, last main pillar of modern gait analysis, usage of EMG electrodes has been worked upon and integrated to the gait analysis. In 21th century gait analysis became the focus in the robotic, therapeutic, medical and sports science [1, 2].

Gait analysis is the method used to define the movement pattern of the human body. In the gait analysis the main features of human walking are identified and quantified. Initially gait analysis is used to understand differences between normal and pathological locomotion. Understanding and discovering abnormalities in the gait cycle helps to discover cause and the treatment of the orthopaedic problems. In the past years gait analysis has also started to be used in the robotics area. Data from gait analysis is used in the designing and the controlling robotics and bionics [3, 1].

Gait analysis consist of four parts: (i) 3D markers and multiple cameras enables

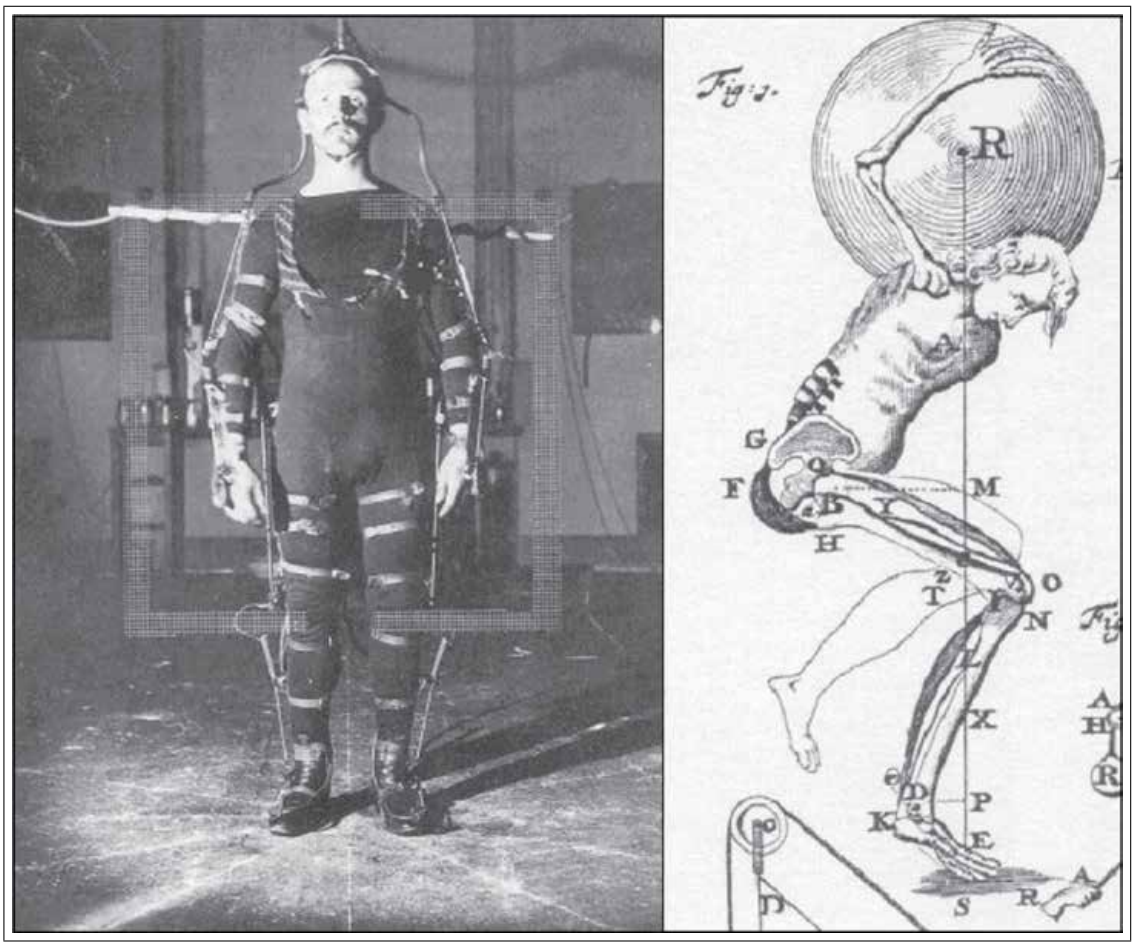

Figure 1.1 On the left subject wearing the experimental suit with the Geisser tubes strapped on it made by Braune and Fischer, on the right Borelli's drawing of a one man standing on toe while bearing a load, which shows his analysis on the human biomechanics [1].

the recording of the movement of the limbs through the gait cycle. (ii) Recording of movement grants us the speed, step width, stride length and angles of the limbs while human walking. (iii) Force plates used in the analysis record the ground force reactions (GFR). (iv) There are electrodes used in the gait analysis alongside with the 3D markers to record the EMG signals from the muscles. In the second part, angle, moment and GRF collected in first part used within the inverse dynamics calculations to estimate the moment and the mechanical power at the limbs [4].

1.1 Significance of Ankle Power

Power generated in the ankle joint is one of the data about the human locomotion provided by the gait analysis [5]. Decrease in the ankle power generation results with the defection in the movement cycle. Reduced step distance in elderly and ankle osteoarthritis patients is linked to power loss in the ankle and knee [6, 7]. In the case of one-sided stroke patients, the side stroke affected loses from its capacity of power generation. The healthy side generates more power to accommodate the affected side. These relations between ankle power and degradation of movement indicate that ankle power identification and estimation and its correlation to gait features is promising for a better understanding of gait abnormalities.

People with lower body amputations spend larger amounts of metabolic energy since they lack net amount of positive ankle power in the amputated limb. This high energy demand makes their mobility range shorter and speed slower. Powered prosthetic aims to provide a net positive push off to prevent this. Timing of such push off support affects the metabolic energy cost [8]. Ankle power is generated right before foot leaves the ground, which indicates that it's the beginning of push off phase [9]. Improved timings of push off support can be determined taking account timings of higher power generation in ankle joints.

As consequence of above listed issues, estimation of ankle power generation is required in improvement and understanding of human mobility. Core method used in estimation of ankle power is clunky [10]. Inverse dynamics is a method estimates ankle power by assuming rest of the body as a rigid structure. While Inverse Dynamics method grants useful information since this calculation is generated with perturbation method, results are calculation of stationary position and assumption of these mathematics would work in the same way while moving. This assumption causes estimation of higher power values than actual value is. Errors in the results are hard to analyse. Finding the source or the amount of the error is hard. inverse dynamics use ground reaction forces, angles and location of the lower body limbs to calculate moment, torque and power at the ankle [11, 12]. Inverse dynamics requires elaborate assessments in the

clinics with the use of motion tracking cameras force plates and costly software which are not easily applicable to real-life practices [13].

1.2 Surface Electromyography

During muscle contraction, electrical signals are generated. Quantification of those signals is referred to as electromyography (EMG). EMG signals are the results of the contraction of the muscles. Ionic flow through the fibres of the muscle membrane generates electrical current. Motor unit is the core functional unit of a muscle. Activation of single muscle fiber of a motor unit is called motor unit action potential (MUAP), which can be recorded by electrode. Muscle contraction is achieved by repeated activation of motor units. These repeated sequence of the MUAPs creates motor unit action potential train. (MUAPT). Linear summation of the MUAPTs results with the EMG signal. Consequently, EMG provides information on the human locomotion. There are four factors that can affect the detection quality of EMG: (1) geometrical relationship between muscle fibers and surface of the electrode, (2) positional relationship between nerve branches of muscle fibers and surface of the electrode (3) size of the muscle fibers and (4) quantity of the muscle fibers of a motor unit in the area where the electrode is placed. EMG data is divided into two groups with regards to the method of electrode placement [14]. Surface EMG (sEMG) is recorded by electrodes located on the surface [15]. Two types of surface electrodes are used to detect sEMG: passive and active electrodes. Passive electrodes are conductive pieces that can detect sEMG through skin surface. Active electrodes consist of high input impedance electronics amplifiers to prevent it to be affected by impedance. sEMG electrodes of preferred type are placed upon skin surface therefore they can monitor the subjects' activity in daily basic tasks with ease [16]. sEMG data have been used in two ways: first is recognition of human motion modes, but only a limited number of modes can be extracted. Second is to use sEMG data to estimate the variables that characterize human locomotion [17]. There have been models developed using sEMG data to estimate gait variables such as lower extremity joint moment by feeding the sEMG data and gait data to deep learning − neural network systems [18].

1.3 Machine learning

Machine learning is replicating the basic capacities of must powerful processor on the earth, i.e., the human brain. Gaining new information, gaining skills and abilities through repeating practices and creating new information and estimation with the scope of observation and experimentation are very hard tasks even though they seem to be very basic for human brain. In order to replicate such capacity by computers the basics of machine learning have been developed. Neural networks are offshoot of the machine learning inspired by human brain neuron structure, used in classification, clustering, pattern recognition and prediction in many disciplines [19].

Machine learning and the neural networks are used in various topics related to human physiology. Implementation of machine learning reduced number of tests, hindered the negative effects of the missing and the noisy data. There are specialized types of neural networks. Recurrent neural network is one the specializations. Recurrent neural networks have shown higher success when using sequential data since RNNs have the ability of passing the information generated in previous sequence to the next. However, in long sequences, information from previous steps has the risk of being more effective than desired or having no effect on the output of the system. Long short-term memory (LSTM) is the RNN model developed to solve problems in long sequences with input and output cells [20, 21, 22, 23].

Models have been proposed to estimate gait related information. L. Zhang et al used EMG data and ankle joint angles as input to the artificial neural network (ANN) to estimate torque at the ankles in the seven movement tasks [24]. Dallali, H et al. also used the EMG as the input to an ANN to estimate the ankle impedance [25]. RNNs have been used in the mechanical variables in the lower body. Zangene AR. et al used RNN structure to estimate kinematics during squat move and H. C. Siu et al developed to estimate ankle torque with sEMG by using RNN structure [26, 27]. Not all previous studies with RNN structure uses EMG as input there is also a model aimed at estimating gait phases with IMUs by RNN structure [28].

The study made by Keles and Yucesoy on prosthesis in the Biomechanics Lab of the Biomedical Engineering Institute of Bogazici University is starting point of the series of studies made in the Bogazici University. Our study is part of the that series of studies. While work done by Keles and Yucesoy developed ANN structure control algorithm and find minimum number of the EMG sensors needed for it to function. They have tested their system with combinations of the muscles and compared the result [29, 30].

In our study, we used dataset collected by Laboratory for Movement Analysis of Biomedical Technology Department of Don Carlo Gnocchi Foundation Scientific Institute of Milano. sEMG data are grouped under the muscles as collected in the publicly accessible dataset [31]. sEMG data were recorded from the dominant side, from the following muscles tibialis anterior (TA), soleus (SO), gastrocnemius medialis (GM), peroneus longus (PL), rectus femoris (RF), vastus medialis (VM), biceps femoris (BF) and gluteus maximus (GMax)[31].

1.4 Muscles and Functions

Functions and the locations of the targeted muscles for sEMG recordings are addressed below. Tibialis anterior is one of the ventral muscles of the lower leg. It has the function of dorsoflexion of ankle joint and supination of foot. Soleus is a part of a muscle structure called triceps surae. It has the function of planar flexion in ankle joint and supination in the intertarsal joints. Gastrocnemius medialis is also a part of triceps surae. It has same functionality with soleus with addition of knee join flexion. Peroneus (fibularis) longus is a lateral muscle in the lower leg, it helps ankle joint flexion and press the foot to inward direction to distribute force upon foot landing (pronation). Rectus femoris and vastus medialis are thigh muscles, which are part of muscle structure called quadriceps femoris and work on the knee joint extensions. Biceps femoris is also thigh muscle, helps knee joint extension and lateral rotation of the knee. Gluteus maximus is a muscle located in hip works on knee extension and hip joint extension, rotation and adduction [32].

Figures 1.2 and 1.3 shows the locations of the muscles on the lower body [33, 32].

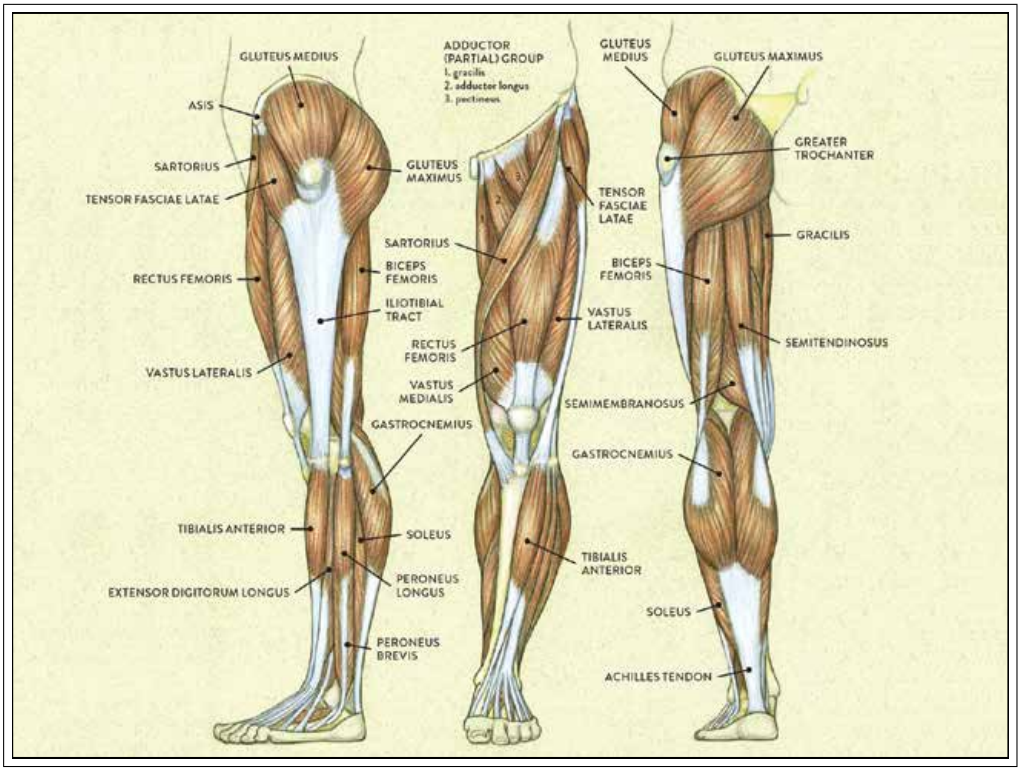

Figure 1.2 Name and the location of the lower and upper leg muscles shown in the (i) lateral (ii) frontal and (iii) posterior view [33].

While the general function of the target muscles are as listed above, throughout level walking movement, these muscles have three main functions: (i) generating support by opposing gravity, (ii) acceleration of body in forward direction (referred to as progression) and (iii) keeping steps on course by controlling mediolateral balance. Muscle functions throughout the walking is characterized by biomechanical measurements and calculations i.e., measurement of ground forces, measurement of body segmented motion and information about loading at muscle and joint contract. Muscles are not performing these functions in a united fashion. While GMax and VM generates supports in the first half of the one-legged stance, GM and SO generates acceleration for the centre of mass. In the beginning of walking VM decelerates the forward speed, in later stage SO and GM accelerates the centre of mass. VM accelerates the body medially while SO and GM accelerates the body laterally. Muscles can perform some functions in synchronized manner. Creating support in early single leg stage, maintaining forward motion in the early stance stage are functions SO and GM perform

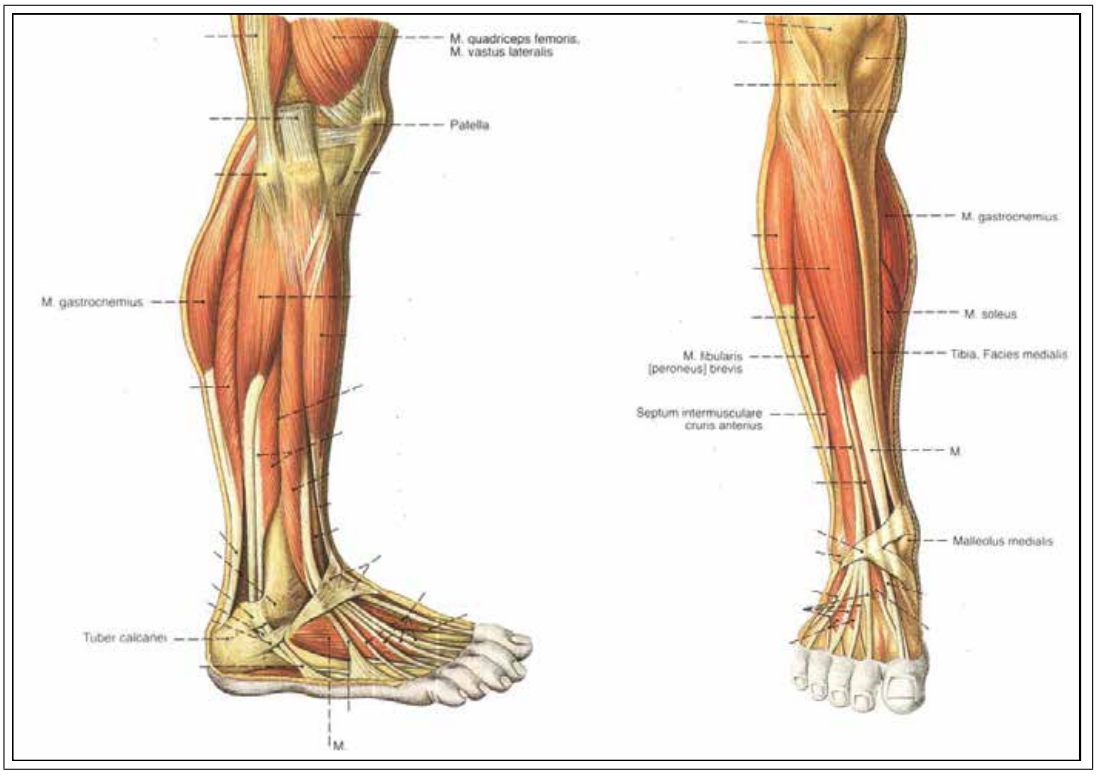

Figure 1.3 Name and the locations of the lower leg muscles in (i) lateral and (ii) frontal view [32].

together and can be shown as example of synchronized work of muscles [34].

1.5 Aims of the Thesis

An improved understanding of the human locomotion has been a historically interesting topic for the scientific circles. Among numerous human walking parameters, ankle power is an important, yet an underutilized variable. A proper estimation of ankle power can allow identification of gait abnormalities and the timing cycle of the foot leaving the ground. However, current methods of estimation of ankle power either assume human body as a rigid structure and yield overestimation or requires a well-equipped lab environment. Nevertheless, sEMG recording can be achieved while subjects daily activities. Once it is trained the RNN structures with sEMG input can estimate the ankle power without the need of high costing equipment like force plates, 3D markers and cameras.

Since the muscles have different functions in the ankle joint while human walking. We hypostasize that training the and testing data with combinations of the muscles would provide higher correlation rather than using all of the muscles at the same time.

the aim in this study is to develop a recurrent neural network based estimation algorith for ankle power by using surface EMG data. In this study, the objectives by utilizing sEMG data of lower extremity muscles coupled with gait analyses data are (1) to build an RNN structure to estimate ankle power during level walking, (2) to train and test the system with the data provided by the Lencioni et al [31] and (3) to test the success of the developed system per all combinations of target muscle groups and to rank those combinations objectively.

2. METHOD

2.1 Dataset

In our study we used dataset obtained by Lancioni et al[31]. This dataset has kinematic, kinetic and EMG data of 50 subjects varied between age of 8-72 (25 male and 25 female subjects). The data set includes no subjects who has disorders in locomotion or motion impairing conditions [31].

Data have been acquired by the Laboratory for Movement Analysis of Biomedical Technology Department of Don Carlo Gnocchi Foundation Scientific Institute in Milano, Italy. The equipments that are used in data acquisition are: a 9-camera motion capture system (SMART system, BTS, Garbagnate Milanese, Italy), two force platforms (Kistler, Winterthur, Switzerland) and a 8-channels wireless EMG recording system (ZeroWirePlus, Cometa, Bareggio, Italy). Equipment used are shown in the Figure 2.2. Hardware was complimented with software that is specialized data accusation of the motion capture systems; SMART Capture, version 1.10, BTS, Italy. The recorded frequencies are for marker trajectories were 60 Hz vs 200 Hz, for force plate data were 800 Hz or 960 Hz, for EMG were 800 Hz, 960 Hz or 1000 Hz. SMART system software has been calibrated on the volume of $5x3x2m^3$. In this system, 3D coordinates of markers have been constructed within the accuracy that is less than 1 mm in every available direction in the calibrated volume [31].

In the beginning of the motion capture, subjects have been asked to be equipped with LAMB total-body marker set with the diameter of 12 mm connected on the head, upper limbs, trunk, pelvis and lower limbs. LAMB marker protocol requires extra 8 markers are connected on great trochanters and medial part of the lower limbs. Markers have been placed at the beginning of the experiment. Figure 2.2 shows locations and types of the 3D markers. Subjects wore swimsuits or tight clothes since markers must be placed upon skin. One of the key components placed upon subjects is pre-amplifed

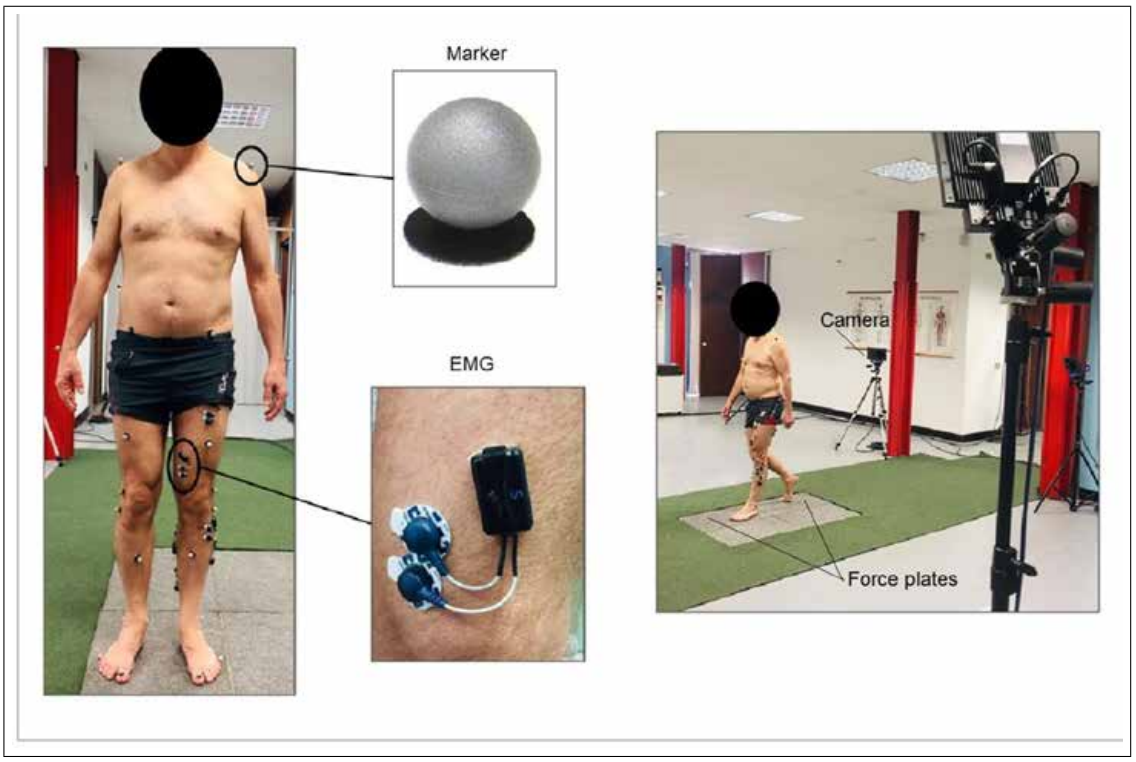

Figure 2.1 Pictures of the equipment used in the data collection; (i) electrodes to collect EMG , (ii) 3D Markers and cameras to record movement in the 3D space on computer and(iii) Force Plate to calculate ground reaction forces [31].

self-adhesive Ag-AgCl electrodes that collects EMG data from muscles [31].

At the next stage of motion capture, the subjects have been asked to perform ground walking task first with their desired normal pace for 5 trials. Subsequently, the subjects have been asked to decrease their speed in next 5 trails and then asked to increase their speed in the last 5 trials [31].

After the data collection process in the next step makers have been labelled according to their location on the subject's body with the SMART Tracker software. Subsequent to clarification of maker location, acquired data is moved to custom designed software within the MATLAB. According to the LAMB model 3D kinematic and dynamic gait data, pelvis orientation angles, hip, knee and ankle joint angles, moments and powers, and 3D coordinates of the body centre of mass have been calculated. These calculated values have been placed in MATLAB file. The EMG data that is collected also inserted in these MATLAB files without any alteration. Figure

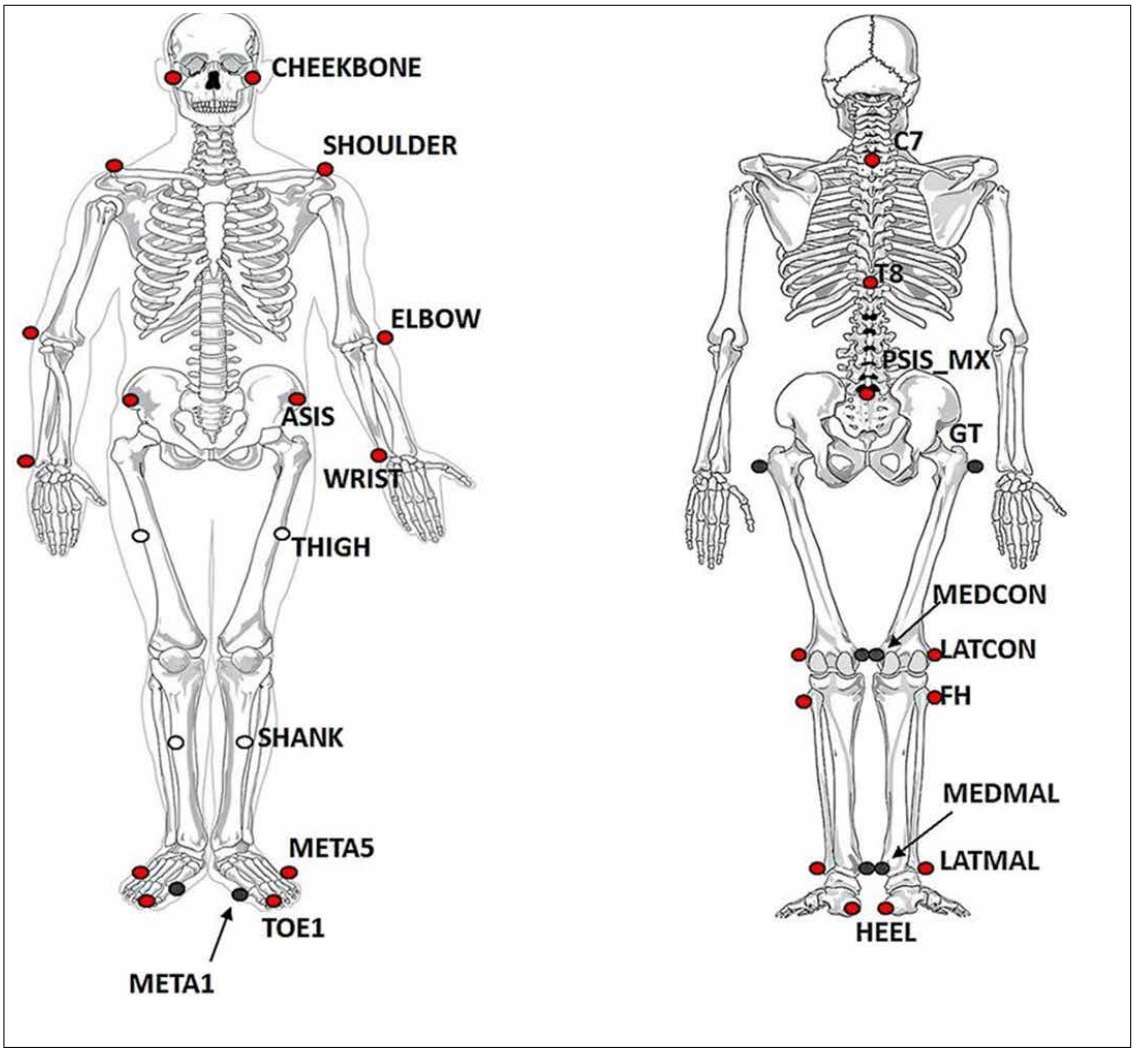

Figure 2.2 Location of the 3D Markers. There are 29 markers presented. 25 Anatomical markers are shown as red dots. 4 Technical markers shown as white dots. Grey dots show the 8 additional anatomical markers, which is used for the calibration. Additional markers are removed after calibration [31].

2.3 shows the flowchart of the data processing [31].

In our study we used EMG sequences and ankle power values to train and test our RNN model.

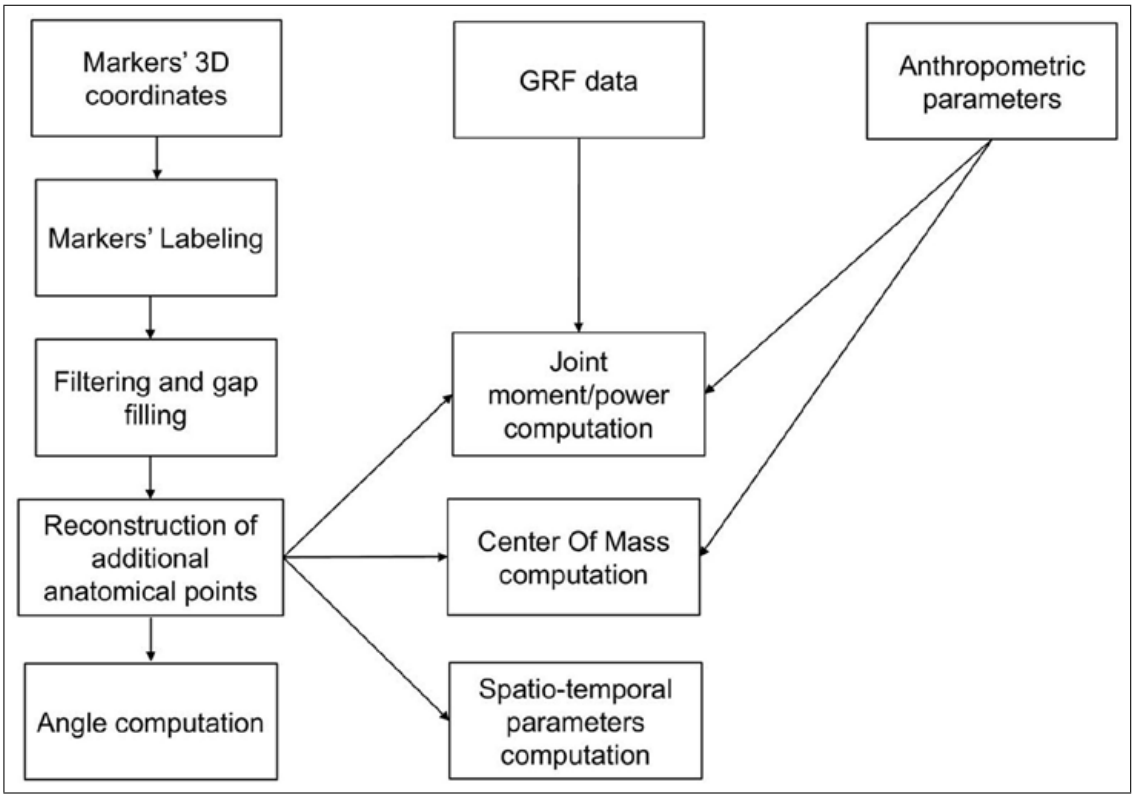

Figure 2.3 Flowchart of the data collection and classification [31].

2.2 Data Pre-processing

2.2.1 Preparing Ankle Power Data to the RNN

In the pre-processing stage, first we normalize ankle power data. Dataset provided by Lancioni et al. requires to be normalized since ankle powers data provided, recorded through in an equal interval, they are sequential data. In this study we used RNN to estimate ankle power with sEMG data. Neural networks need data normalization when using sequential data to generate reliable results. Normalization is the scaling of dataset with large value domain to into a scale that has small values as range. Value range of the data that has been fed to the neural network effects the speed of the estimation process therefore we normalized our dataset to increase speed and accuracy of RNN. We used Min-Max normalization method in this study. This method can be explained as all the values in data being placed in between 1 and 0 while maximum value (MaxX) in the dataset assigned as 1 and minimum value (MinX) in the dataset

assigned as 0. Rest of the values are assigned with a decimal in the range of [0,1] by their relation to MaxX and MinX [35, 36].

referred to as Eq. 2.10.

$$Xnorm = \quad ((high - low) * (x - minX))/(maxX - MinX) \tag{2.1}$$

2.2.2 sEMG Smoothing

Since the EMG data is the summation of the multiple MUAPs the EMG signals have noises, spikes interfering the useful data. Interference can be described as the multiple domains residing in the sequential dataset [37]. sEMG dataset have frequency domain and the time domain inside. We used the time domain feature in the SEMG data. Previous research showed that when extracting frequency domain from sequential data there is significant loss of data. Additionally, time domain feature requires less computing time and gave much successful results when EMG data used as a input of a neural network systems [38, 39, 40].

We have used moving average filtering (MAF) to extract the time domain from the raw EMG data. Smoothing the EMG data with the MAF used in the previous systems used EMG data as input in the understanding and estimating the gait related features [41, 42, 43]. MAF achieved in MATLAB by using the smooth command with the span of 10. Mathematics of the MAF in the MATLAB can described as bellow.

$$y_{(s)(\mathrm{i})=}(1/2N+\ 1)\,(y\,(i+N)+y\,(i+N-1)+\ldots+y\,(i-N)) \tag{2.2}$$

y_s (i) denotes the smoothed value while 2N+1 is span, N is the number of neighbouring data.

In the next part of the pre-processing of the sEMG data we interpolated the smoothed EMG data to have the EMG data length equal to ankle power data length. The equalization oif the length in needed to RNN features to work in the MATLAB.

Muscles in the dataset we have used in this study, perform different functions in the different stages of ground walking. Therefore, we created muscle sets. sEMG data in the dataset are collected from 8 different muscles in the lower body [31]. Each muscle's sEMG data is provided as been grouped under the name of the muscle they are collected. Muscle sets are the random combinations of these muscle groups .

2.3 Recurrent Neural Network

2.3.1 Creation of Neural Network

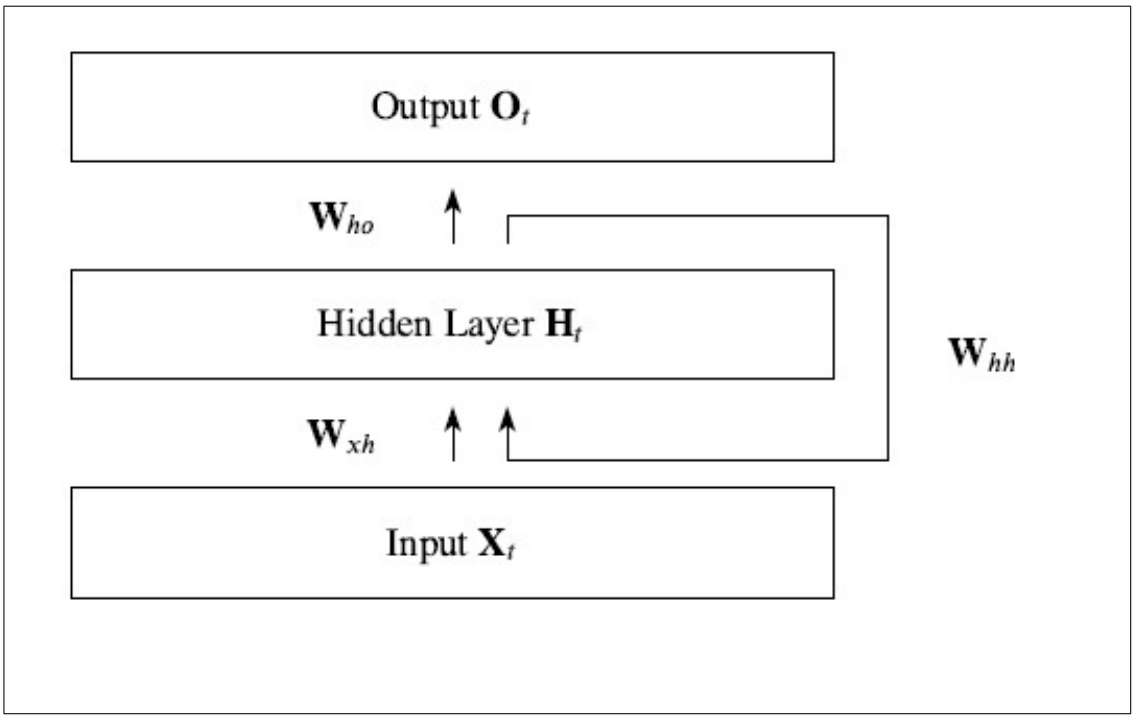

Figure 2.4 Basic Recurrent Neural Network structure [44].

In this study, we developed a recurrent neural network system to estimate ankle power with relation to sEMG. Recurrent neural network is used since this structure

type have been accepted to much more effective on sequential data. Basic representation of the RNN is shown in the Figure 2.4. In RNN structure information that is created through the neural network is fed back to the next node of the neural network. Mathematics of the structure we used can be described as follows:

$$H_t = \varphi_h(X_t W_{xh} + H_{t-1} W_{hh} + b_h \tag{2.3}$$

$$O_t = \varphi_o(H_t W_{hO} + b_O) \tag{2.4}$$

O_t denotes is the output at the time step t. $H_t^{n\ x\ h}$ denotes the hidden state at the time step t and $X_t^{n\ x\ d}$ denoted the input at the time step t. Number of samples is n, number of inputs is d and number of hidden units is h. $W_{xh} \in R^{d\ x\ h}$ is the weight matrix, $W_{hh} \in R^{h\ x\ h}$ is hidden-state-to-hidden-state matrix. Bias parameter have been shown as $b_h \in R^{1\ x\ h}$. φ is the function that all the info created previously has passed in. this function creates gradients in the backpropagation process of RNN[44].

We used Long Short − Term Memory Units (LSTMs) for prevention of vanishing or exploding gradients. Through gated cells in LSTM, RNN structure we created stores high density of data outside of the flow of neural network. In LSTM structure, there is a control layer, which is non-linear and data dependent, that is trained to keep gradient relevant regards to state signal. Figure 2.5 shows diagram of connections of gate cells and memory cells inside a RNN structure [44].

Mathematical description of LSTMs includes the description of the cells that hold the information:

$$O_t = \varphi(X_t W_{xo} + H_{t-1} W_{ho} + b_o) \tag{2.5}$$

$$I_t = \varphi(X_t W_{xi} + H_{t-1} W_{hi} + b_i) \tag{2.6}$$

$$F_t = \varphi(X_t W_{xf} + H_{t-1} W_{hf} + b_f) \tag{2.7}$$

O_t is output gate, I_t is input gate and F_t is forget gate.

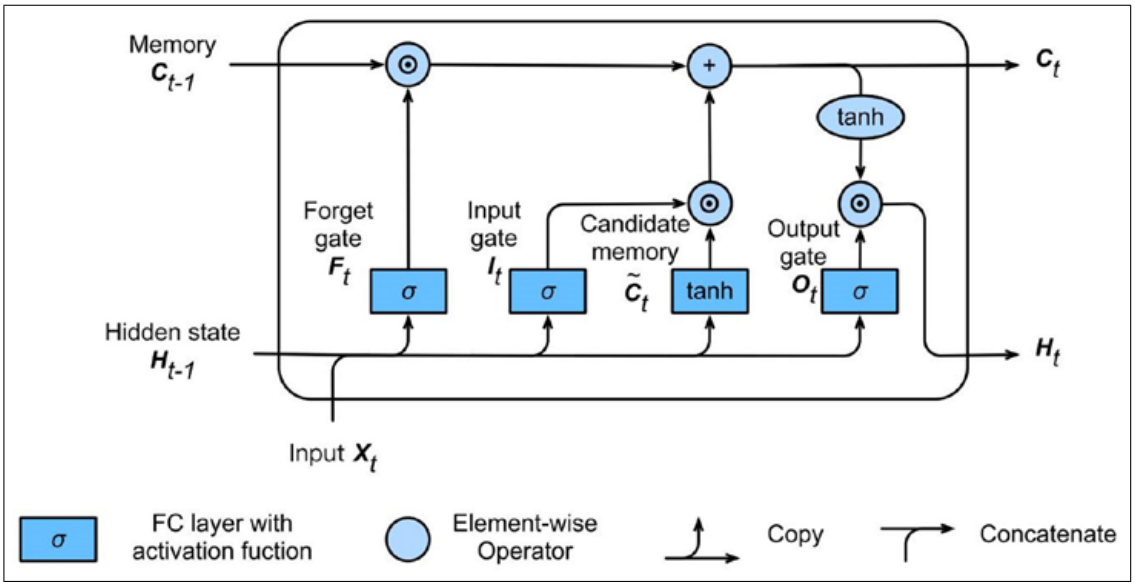

Figure 2.5 Recurrent Neural Network diagram showing the connections gate cells and memory cells [44].

In the next step, we choose a candidate memory cell, which uses a tanh function for activation. Tanh function prevents having an output value lower than -1 and higher than 1.

Memory cell is denoted with C_t.

$$C_t = tanh(X_t W_{xc} + H_{t-1} W_{hc} + b_c) \tag{2.8}$$

With the usage of old memory cell content C_{t-1} we try to determinate how much of the information inside the memory cell should be kept using in next step [44]

2.3.2 Structure of RNN

Presently, the neural network was built upon 6 layers: (i) Input Layer, (ii) LSTM Layer, (iii) Fully Connected Layer, (iv) Dropout Layer, (v) Fully Connected Layer and (vi) Regression Layer. Input Layer (or as it was written in MATLAB Sequence Input Layer), in the layer where chosen sequential data, which is EMG in this study, fed to the system. LSTM Layer is trained on the correlation between input from previous state and input that comes from sequential data, and it is also trained to keep input from previous steps relevant. Fully Connected Layer is layer where main neural network functions occur which can be summarized as multiplication of input from sequential data with weight matrix. Then result is added to a bias vector. Purpose of Dropout Layer is prevention of overfitting. This layer has given probably of 0.4 to set some random neurons to zero. At the end regression task's half-mean-squared-error loss determinate in Regression Layer [45].

2.4 Evaluation

In the testing process we have used 80 percent of the data chosen to feed to the RNN is used for training of the system and 20 percent of the data is used for the testing. Success of the study relies upon the correlation between estimated ankle power values and parts of ankle power values we chosen to test, provided by the Lencioni et al. In this study two statistics test used to determinate the performance: Pearson's correlation coefficient (r). and Root mean square error (RMSE). Pearson Correlation. Pearson Correlation is a measurement method linear relation between two variables.

$$\mathrm{r} \ =(x-x)(y-{}^{3})(x-x)2(y-{}^{3})2 \tag{2.9}$$

The x denotes the predictions made by the system and the y denotes the test

data values. Summation of the squared differences between the predicted data and the test data gives the mean square error. Root of the mean square error is the RMSE value.

$$\text{RSME} = \sqrt{\sum_{t=1}^{n} \frac{(x_t - y_t)^2}{\text{n}}} \tag{2.10}$$

Figure 2.6 shows meanings of the size of Pearson's correlation coefficients. If coefficient is between .7 and .9 that indicates strong correlation between two values. If correlation coefficient is higher than .9 that indicates very strong correlation between two values. In our study, correlation means the similarity between ankle power values generated by the RNN structure and the ankle power values provided by Lencioni et al. In our study, if testing of muscle set results with correlation coefficient higher than .9. we accept that system is successful with that muscle set [46, 47].

Size of Correlation	**Interpretation**
.90 to 1.00 (-.90 to –1.00)	Very high positive (negative) correlation
.70 to .90 (-.70 to -.90)	High positive (negative) correlation
.50 to .70 (-.50 to -.70)	Moderate positive (negative) correlation
.30 to .50 (-.30 to -.50)	Low positive (negative) correlation
.00 to .30 (.00 to -.30)	negligible correlation

Figure 2.6 Relations of between the Size of Correlation and Interpretation [47].

3. RESULTS

Results are presented in this section. Test data and training data distributions are randomized to prevent possible biases can be caused by handmade distribution.

Table 3.1 show the muscle sets with the successful predictions. PL and GM muscles presented frequently among the successful muscle sets. Both PL and GM are presented in the 21 out of 25 muscle sets and there are only 2 muscles sets don't have neither GM or PL. in the Table 3.1 that does not include either PL or GM.

Table 3.1
Shows the successful muscle sets.

Muscle Set	Pearson's Correlation Coefficient (r)	RMSE
PL-GM-RF-VM-GMax	0.9567914	0.06539075
PL-GM-RF-VM	0.9551548	0.09204038
PL-GM-BF-RF-VM-GMax	0.9531613	0.06238307
PL-GM-VM	0.9510835	0.06882809
TA-GM	0.9486784	0.0998422
PL-GM	0.9464687	0.09405731
PL-GM-VM-GMax	0.9463876	0.08528634
PL-TA-GM-VM	0.9412125	0.08130904
PL-GM-BF-VM	0.9393917	0.09224925
TA-RF-GMax	0.9388932	0.1155776
PL-GM-BF	0.9379611	0.07725865
PL-TA-GM-BF-GMax	0.9362692	0.09133928
GM	0.9361292	0.09366534
PL-TA-GM-GMax	0.9347829	0.1184108
PL-TA-GM-BF-RF-VM-GMax	0.9326558	0.08539473
PL-TA-GM-RF-GMax	0.9279891	0.08651469
PL-TA-GM	0.9251679	0.1014929
PL-TA-GM-BF	0.9217342	0.08626757
TA-BF-RF	0.9182746	0.1082933
PL-TA-GM-BF-VM	0.9140787	0.08352283
PL-GM-BF-GMax	0.9100521	0.09301141
PL-GM-BF-RF-VM	0.9087852	0.1002395
PL-GM-RF-GMax	0.9087607	0.1144778
PL-GM-BF-RF	0.9058505	0.1062211
PL-TA	0.9024382	0.1066816

4. DISCUSSION AND CONCLUSION

Estimation of the ankle power in human walking with usage of the sEMG data was the objective of this study. Estimation method proposed relies upon three main features; it (i) takes ankle power data obtained from gait analyses of numerous participants as the reference, (ii) uses RNN structure to estimate ankle power, by (iii) using solely sEMG data of all combinations of numerous lower extremity muscles. As a result, an RNN structure yielding ankle power estimation algorithms was developed which is capable of providing high correlation predictions with real data.

Functions of muscles during walking have similarities and differences. In this study we tested all possible muscle combinations of the muscles for which sEMG data were included the open-source dataset [31]. We assessed to find and understand if successful combinations have recurring muscles and if there are any similarities in the functions of these muscles. Muscles with ankle planar flexion function have the highest representation in the successful muscle sets. Out of 25 successful muscle sets only 2 of them did not have PL and GM. Other successful muscle sets either included PL and GM or both. Particularly GM but also PL has the function of planar flexion in the ankle [32].

Research has been conducted on human locomotion that used ANNs to predict ankle moment, ankle torque and ankle angles. The system proposed by Senanayake and co-workers converts IMU data to ankle join angle by using deep neural networks [48]. In the study conducted by Hahn and O'Keefe, an ANN system was developed to estimate lower extremity joint moments [49]. Jiang et al. proposed a system that uses data from IMUs with machine learning to estimate ankle power [13]. These examples show that even though usage of ANN to estimate gait data including ankle power has been done previously, the use of an RNN structure with sEMG data to estimate ankle power as was used in this study is a new approach.

The control algorithms developed by Keles and Yucesoy [29, 30] in the Biomechanics Lab of the Biomedical Engineering Institute of Bogazici University is a beginning point also for this study. Those authors developed a neural network system to estimate ankle moment and position with the utilization of the least number of the sEMG sensors in order to develop control algorithms for powered prosthetic devices. Our study can supplement their approach since both studies aim to address the need for developing precise powered prosthetic devices cost-effectively. Their study provides the moment and the position estimation in real time, which can be used in the calculations of net positive power needed for push off while our study can provide the correct timing for the net positive power generation since ankle power reaches a peak at the push off phase of walking. With the right timing of push offs in the powered prosthetics, metabolic energy spent by the patient will be reduced [8, 50, 29, 30] .This can also allow for optimizing battery use or even facilitate development of novel battery technologies for such devices and further help cost-effectiveness.

Note that, there are differences in muscle contents of successful muscle combinations between our study and the study by Keles and Yucesoy [29, 30] . In their study goal was to keep the number of the sEMG sensors needed to operate a powered ankle prosthetics. GMax + BF + GM is one of the successful muscle sets in their study with least number of lower leg muscle. Lesser amount of lower leg muscles would increase the number of patients that system can be implemented on. In our study GM muscle is one of the two most frequent muscles. Even using only data from GM yields successful result in our study with r = 0.93 but in the work of Keles success threshold is set at r $>$ 0.95. Further works might have the goal of having r $>$ .95 with one of the GMax, BF and GM muscles or combinations of them to get in line with the Yucesoy and Keles.

Since ankle power is indicator for muscle performance and capacity, in traditional gait analysis it is used for diagnostics and rehabilitation [6, 7]. As stated above current methods for ankle power estimation needs data from gait analysis labs with specialized equipment and long preparation times [13]. Our system has successfully estimated ankle power at the healthy subjects therefore our system can be a faster and cheaper method for the diagnostics and rehabilitation. Further studies might test this

system with non-healthy subjects to increase the viability of our system as a clinical method.

In our study we used moving average filtering for the removing the noise of the sEMG data. In future studies and application, the other methods for the sEMG filtering can be tried to increase the number of successful muscle sets.

In conclusion, our study showed that using RNN with only sEMG as sensor data is a good approach to estimate ankle power during level walking of healthy individuals. Our study indicated that GM muscle provides successful estimations with the use of a minimum number of sEMG sensors. New studies are indicated to implement this method to other forms of human motion including inclined surface walking and stair ascend and descend movements.

APPENDIX A. APPENDIX

A.1 All Muscle set Results

Tables A.1 to A.11 shows the results from all muscle sets generated for this study.

Table A.1
Shows the results from all muscle sets.

Muscle Set	Pearson's Correlation Coefficient (r)	RMSE
PL-GM-RF-VM-GMax	0.9567914	0.06539075
PL-GM-RF-VM-GMax	0.9567914	0.06539075
PL-GM-RF-VM	0.9551548	0.09204038
PL-GM-BF-RF-VM-GMax	0.9531613	0.06238307
PL-GM-VM	0.9510835	0.06882809
TA-GM	0.9486784	0.0998422
PL-GM	0.9464687	0.09405731
PL-GM-VM-GMax	0.9463876	0.08528634
PL-TA-GM-VM	0.9412125	0.08130904
PL-GM-BF-VM	0.9393917	0.09224925
TA-RF-GMax	0.9388932	0.1155776
PL-GM-BF	0.9379611	0.07725865
PL-TA-GM-BF-GMax	0.9362692	0.09133928
GM	0.9361292	0.09366534
PL-TA-GM-GMax	0.9347829	0.1184108
PL-TA-GM-BF-RF-VM-GMax	0.9326558	0.08539473
PL-TA-GM-RF-GMax	0.9279891	0.08651469
PL-TA-GM	0.9251679	0.1014929
PL-TA-GM-BF	0.9217342	0.08626757
TA-BF-RF	0.9182746	0.1082933
PL-TA-GM-BF-VM	0.9140787	0.08352283
PL-GM-BF-GMax	0.9100521	0.09301141
PL-GM-BF-RF-VM	0.9087852	0.1002395
PL-GM-RF-GMax	0.9087607	0.1144778
PL-GM-BF-RF	0.9058505	0.1062211
PL-TA	0.9024382	0.1066816

Table A.2
Continuation of Table A.1.

Muscle Set	Pearson's Correlation Coefficient (r)	RMSE
PL-GM-BF-RF-GMax	0.8957897	0.1125354
PL-TA-RF	0.8932867	0.1003098
TA-GM-BF	0.8918099	0.1171125
PL-TA-GM-RF	0.8898363	0.1153123
PL-BF-RF	0.8837346	0.09976094
TA-GM-BF-RF	0.8833618	0.1070685
PL-BF	0.8832132	0.1131728
GM-BF-RF	0.8831369	0.1182125
PL-TA-GM-BF-RF-GMax	0.8825469	0.1218626
PL	0.8812568	0.1029814
TA-BF-RF-VM-GMax	0.8775438	0.1119627
PL-GM-RF	0.8709219	0.1125214
PL-GM-BF-VM-GMax	0.8686955	0.1070919
TA-GM-VM-GMax	0.8562585	0.1390722
PL-TA-GM-BF-RF-VM	0.851771	0.1150993
PL-TA-GM-RF-VM-GMax	0.8504697	0.1108527
PL-SO-GM	0.8368479	0.1145153
SO-GM	0.8354242	0.1191968
PL-GM-GMax	0.8318044	0.1369342
TA	0.8278097	0.1215823
PL-TA-GM-RF-VM	0.8184122	0.1342801
PL-SO-GM-RF-GMax	0.8111691	0.120126
RF	0.8032812	0.1564077
TA-BF	0.7997373	0.1398855
PL-SO-TA-GM-VM	0.7885997	0.1269888
PL-SO-GM-RF-VM-GMax	0.7881715	0.1353678

Table A.3
Continuation of Table A.1.

Muscle Set	Pearson's Correlation Coefficient (r)	RMSE
PL-SO-TA-GM-GMax	0.7623091	0.1401075
PL-SO-TA-GM-BF-VM-GMax	0.7587984	0.140015
PL-SO-GM-BF-RF-GMax	0.7479325	0.1347764
PL-SO-TA-GM-RF-VM-GMax	0.7476196	0.1355023
PL-SO-TA-GM-RF-VM	0.7466552	0.1361065
PL-SO-GM-BF-VM	0.7447623	0.1747064
PL-SO-GM-BF-GMax	0.7434628	0.1404287
PL-TA-GM-VM-GMax	0.7426981	0.1557025
PL-SO-GM-BF-VM-GMax	0.7399783	0.1381393
SO-TA-GM	0.7398418	0.151173
PL-SO-GM-BF-RF-VM-GMax	0.7329865	0.1389637
PL-TA-GM-BF-VM-GMax	0.7299543	0.1472808
SO-TA-BF-VM	0.7138654	0.1769742
SO-TA	0.7091292	0.1461309
PL-SO-TA-GM-BF	0.7071196	0.1477083
PL-SO-GM-GMax	0.7069803	0.1468983
PL-SO-TA	0.706055	0.1500543
PL-SO-TA-GM-RF-GMax	0.7023551	0.1582934
PL-SO-GM-VM-GMax	0.7018826	0.1471985
SO-BF-VM	0.7004145	0.1750527
SO	0.6975193	0.1687169
PL-BF-VM-GMax	0.6915361	0.1567349
PL-SO-TA-GM-VM-GMax	0.6869183	0.1491759
PL-SO-TA-GM-BF-RF-GMax	0.6707251	0.1534858
PL-SO-GM-BF-RF-VM	0.6706446	0.1613267
SO-TA-BF-RF-VM-GMax	0.6687875	0.2059681

Table A.4
Continuation of Table A.1..

Muscle Set	Pearson's Correlation Coefficient (r)	RMSE
PL-SO-TA-GM-BF-RF-VM	0.668189	0.1568669
SO-TA-VM	0.6627873	0.1907705
SO-TA-VM-GMax	0.6470042	0.1646492
PL-SO-TA-GM	0.6408311	0.1708209
PL-SO-GM-RF-VM	0.6373127	0.1689272
SO-TA-GM-VM-GMax	0.6314917	0.1604589
PL-SO-GM-VM	0.6300455	0.1676966
PL-SO	0.6257985	0.1613387
SO-TA-GM-BF-VM	0.6174242	0.180181
SO-VM-GMax	0.6061841	0.1878672
PL-SO-TA-BF-RF-VM-GMax	0.6046128	0.1653769
SO-GM-VM	0.6031212	0.1927273
PL-SO-TA-GMax	0.6027539	0.1644983
SO-BF-RF-VM-GMax	0.6022845	0.1851097
SO-BF-RF-GMax	0.6003848	0.1858716
PL-SO-BF-RF-GMax	0.5982868	0.1674324
PL-SO-TA-BF-VM	0.5979238	0.1671227
PL-SO-GM-RF	0.5953131	0.1773452
SO-TA-GM-VM	0.5948197	0.2083275
PL-SO-TA-RF-VM-GMax	0.5939366	0.1897221
PL-SO-VM-GMax	0.5891236	0.1675627
SO-TA-RF	0.584381	0.2017039
PL-SO-BF-GMax	0.5812652	0.1764566
PL-SO-TA-BF-RF-GMax	0.5774316	0.1762402
SO-TA-GM-BF-RF-GMax	0.5702333	0.1753472

Table A.5
Continuation of Table A.1.

Muscle Set	Pearson's Correlation Coefficient (r)	RMSE
SO-GM-RF-GMax	0.5662297	0.1800466
SO-TA-GM-RF-VM-GMax	0.5659832	0.1879896
SO-TA-BF-VM-GMax	0.5637038	0.1699629
PL-SO-TA-VM-GMax	0.5603715	0.1719561
SO-TA-RF-VM	0.5600524	0.1794834
SO-BF-GMax	0.558313	0.1894712
SO-GM-GMax	0.55663	0.1783881
PL-SO-TA-BF-RF-VM	0.5538519	0.1687575
SO-TA-RF-GMax	0.5515347	0.1712507
PL-SO-VM	0.5485253	0.1897759
PL-SO-TA-VM	0.5484263	0.1845668
SO-GM-VM-GMax	0.5454023	0.1868817
SO-RF-GMax	0.5444608	0.1882551
PL-SO-TA-GM-RF	0.5416347	0.1742651
SO-GM-BF-RF-GMax	0.5325745	0.2490838
SO-GM-BF-VM-GMax	0.531989	0.1891857
SO-TA-GM-GMax	0.5266477	0.2018559
SO-VM	0.5256709	0.1824276
SO-BF-VM-GMax	0.5209076	0.178845
SO-GMax	0.5169911	0.1980862
PL-SO-RF-VM-GMax	0.5166778	0.2077032
SO-GM-BF-RF-VM	0.5152727	0.1840511
SO-GM-BF-GMax	0.5140051	0.2212451
SO-GM-BF	0.5090771	0.1776
SO-GM-RF-VM-GMax	0.5003521	0.2012727

Table A.6
Continuation of Table A.1.

Muscle Set	Pearson's Correlation Coefficient (r)	RMSE
SO-TA-GM-RF-GMax	0.497997	0.1936216
SO-TA-GM-BF	0.4972169	0.2222521
PL-SO-BF-VM-GMax	0.4928957	0.2049985
PL-SO-TA-GM-BF-RF	0.4925721	0.2116725
PL-SO-TA-BF-RF	0.4906014	0.217672
SO-TA-GM-BF-VM-GMax	0.4872321	0.2078336
PL-TA-BF-RF	0.4847238	0.2076134
SO-GM-RF-VM	0.4828797	0.1950419
SO-TA-BF-GMax	0.481719	0.2024854
PL-SO-TA-BF-GMax	0.4804336	0.1993706
PL-TA-GM-BF-RF	0.4789793	0.1909123
PL-SO-TA-GM-BF-RF-VM-GMax	0.4772522	0.2537943
SO-TA-GM-RF-VM	0.4768503	0.1847091
PL-SO-BF-RF-VM	0.4644236	0.1896378
SO-TA-GM-BF-RF	0.4607728	0.2566226
TA-GMax	0.4591639	0.1992044
SO-RF-VM	0.4582309	0.188707
SO-TA-BF-RF-VM	0.4563319	0.2115626
SO-TA-BF-RF-GMax	0.4462135	0.2632475
PL-SO-GM-BF-RF	0.4458957	0.2407224
PL-SO-TA-RF-GMax	0.4358754	0.2196225
PL-SO-RF	0.4286568	0.215456
PL-SO-TA-RF	0.4262018	0.2284104
SO-RF-VM-GMax	0.4220304	0.1862913
SO-TA-GM-RF	0.4175747	0.2564294

Table A.7
Continuation of Table A.1.

Muscle Set	Pearson's Correlation Coefficient (r)	RMSE
SO-TA-BF	0.4165753	0.2392493
SO-TA-BF-RF	0.4144772	0.2443156
PL-SO-TA-GM-BF-VM	0.3971452	0.2189479
PL-SO-TA-BF	0.3932461	0.2228237
SO-GM-BF-VM	0.3881855	0.221737
SO-RF	0.3767655	0.2686983
SO-BF-RF-VM	0.3676541	0.2194509
SO-BF-RF	0.3621478	0.2097944
SO-GM-BF-RF	0.3493257	0.2850876
PL-SO-BF-RF	0.3487795	0.2656755
PL-SO-RF-VM	0.3426046	0.2265815
SO-TA-GM-BF-GMax	0.3407623	0.211553
SO-TA-RF-VM-GMax	0.3311969	0.2543895
PL-SO-TA-BF-VM-GMax	0.3178611	0.2320089
PL-SO-RF-GMax	0.3176571	0.2521977
GM-BF-VM-GMax	0.307849	0.1990507
GM-VM-GMax	0.3058016	0.2096819
BF	0.2993796	0.1988278
PL-SO-BF	0.2987478	0.2643662
SO-GM-RF	0.2820088	0.2649736
SO-TA-GM-BF-RF-VM	0.2782172	0.2189786
PL-SO-GM-BF	0.2344523	0.2282877
PL-TA-BF	0.2250222	0.2018353
PL-VM-GMax	0.2150956	0.2076398
PL-RF-VM-GMax	0.2116415	0.202937

Table A.8
Continuation of Table A.1.

Muscle Set	Pearson's Correlation Coefficient (r)	RMSE
GM-BF	0.2059336	0.2008032
GM-RF	0.2036895	0.2000167
PL-RF-GMax	0.2015875	0.1991407
GM-RF-VM-GMax	0.201243	0.2113001
TA-BF-VM-GMax	0.1976941	0.1998039
PL-RF	0.1942094	0.1987525
PL-TA-BF-RF-GMax	0.1925732	0.1992501
PL-TA-RF-GMax	0.1914031	0.2034499
GM-RF-GMax	0.1913458	0.1989407
PL-TA-VM-GMax	0.1897312	0.2015125
BF-RF	0.1882261	0.2010292
TA-GM-BF-GMax	0.1850051	0.1998941
TA-RF	0.1847595	0.2030568
RF-VM-GMax	0.1847441	0.2003517
PL-BF-RF-GMax	0.1816455	0.1991339
TA-GM-RF-VM-GMax	0.1807828	0.2004937
TA-GM-BF-VM-GMax	0.1757337	0.199407
TA-GM-BF-RF-GMax	0.1749944	0.2062646
PL-TA-BF-VM-GMax	0.1748334	0.2009845
TA-GM-BF-RF-VM-GMax	0.1719344	0.2016148
GM-BF-GMax	0.1699104	0.1986723
TA-RF-VM-GMax	0.1697491	0.1995569
BF-RF-VM-GMax	0.1692322	0.1993862
PL-GMax	0.1678089	0.2005723
BF-VM	0.1669545	0.1989612

Table A.9
Continuation of Table A.1.

Muscle Set	Pearson's Correlation Coefficient (r)	RMSE
BF-RF-GMax	0.16673	0.200326
TA-VM-GMax	0.1645217	0.1990101
BF-GMax	0.1637353	0.2005153
TA-GM-GMax	0.1622919	0.2005566
RF-GMax	0.160583	0.2020649
VM-GMax	0.1588777	0.19905
PL-VM	0.1583205	0.1999
PL-BF-GMax	0.1583093	0.1994749
PL-BF-RF-VM-GMax	0.1564523	0.1993069
PL-TA-RF-VM-GMax	0.1535497	0.2058101
PL-TA-RF-VM	0.1519961	0.1992207
VM	0.1490061	0.1995777
PL-SO-TA-RF-VM	0.145151	0.2336761
TA-GM-VM	0.1429568	0.2152808
GM-BF-RF-GMax	0.1379353	0.201355
PL-SO-BF-VM	0.1357353	0.2417784
GM-BF-RF-VM-GMax	0.1352278	0.2068781
TA-GM-RF-VM	0.1349328	0.2098003
TA-RF-VM	0.1262073	0.2070921
TA-GM-RF-GMax	0.1143707	0.2179736
PL-TA-BF-GMax	0.1134649	0.2398836
TA-BF-GMax	0.1086427	0.2066248
PL-BF-RF-VM	0.1038851	0.2077597
PL-SO-GMax	0.1032759	0.2401498
TA-GM-BF-VM	0.09733473	0.2022856

Table A.10
Continuation of Table A.1.

Muscle Set	Pearson's Correlation Coefficient (r)	RMSE
RF-VM	0.09664863	0.2027965
TA-GM-BF-RF-VM	0.09661198	0.2073698
TA-BF-RF-GMax	0.07182215	0.204814
PL-RF-VM	0.06429001	0.203758
GMax	0.05861988	0.2079257
PL-TA-BF-RF-VM-GMax	0.05449744	0.3073804
PL-SO-BF-RF-VM-GMax	0.05430833	0.2183619
GM-VM	0.05394136	0.2019676
GM-BF-RF-VM	0.05372024	0.2034299
TA-VM	0.0520376	0.2020381
TA-BF-RF-VM	0.0518649	0.2017311
GM-RF-VM	0.04743412	0.2043795
BF-RF-VM	0.04520552	0.2017232
GM-BF-VM	0.03974703	0.2016062
PL-TA-BF-VM	0.03266599	0.2022384
PL-TA-BF-RF-VM	0.0304889	0.2032186
PL-TA-VM	0.0277769	0.2029892
TA-BF-VM	0.02228904	0.2085885
PL-SO-TA-GM-BF-GMax	0.01437056	0.2919377
PL-BF-VM	0.008521412	0.2026925
SO-TA-GMax	-0.01537937	0.2289573
PL-TA-GMax	-0.03166211	0.2348864
SO-BF	-0.06106725	0.2903835
SO-GM-BF-RF-VM-GMax	-0.1267457	0.3192861
TA-GM-RF	-0.1577778	0.213166

Table A.11
Continuation of Table A.1.

Muscle Set	Pearson's Correlation Coefficient (r)	RMSE
-VM-GMax	-0.1802233	0.3051485
GM-GMax	-0.1871284	0.2724983
SO-TA-GM-BF-RF-VM-GMax	-0.2161513	0.2774093

REFERENCES

1. Akhtaruzzaman, M., A. A. Shafie, and M. R. Khan, "Gait Analysis: Systems, Technologies, and Importance," *J. Mech. Med. Biol.*, Vol. 16, no. 7, 2016.

2. Baker, R., "The history of gait analysis before the advent of modern computers," *Gait Posture*, Vol. 26, no. 3, 2007.

3. Kyriazis, V., "Gait analysis techniques," *J. Orthop. Traumatol.*, Vol. 2, no. 1, 2001.

4. Baker, R. W., *Measuring Walking: A Handbook of Clinical Gait Analysis.* 2013.

5. Gage, James R.; Deluca, Peter A.; Renshaw, T. S., "Gait Analysis : Principles and Applications," *J. BONE Jt. Surg.*, Vol. 77 A, no. 10 october, 1995.

6. Judge, J. O., R. B. Davis, and S. Öunpuu, "Step length reductions in advanced age: The role of ankle and hip kinetics," *Journals Gerontol. - Ser. A Biol. Sci. Med. Sci.*, Vol. 51, no. 6, 1996.

7. Valderrabano, V., B. M. Nigg, V. von Tscharner, *et al.*, "Gait analysis in ankle osteoarthritis and total ankle replacement," *Clin. Biomech.*, Vol. 22, no. 8, 2007.

8. Malcolm, P., R. E. Quesada, J. M. Caputo, and S. H. Collins, "The influence of push-off timing in a robotic ankle-foot prosthesis on the energetics and mechanics of walking," *J. Neuroeng. Rehabil.*, Vol. 12, no. 1, 2015.

9. Lipfert, S. W., M. Günther, D. Renjewski, and A. Seyfarth, "Impulsive ankle push-off powers leg swing in human walking," *J. Exp. Biol.*, Vol. 217, no. 8, 2014.

10. Zelik, K. E., and E. C. Honert, "Ankle and foot power in gait analysis: Implications for science, technology and clinical assessment," *J. Biomech.*, Vol. 75, 2018.

11. Hansen, A. H., D. S. Childress, S. C. Miff, S. A. Gard, and K. P. Mesplay, "The human ankle during walking: Implications for design of biomimetic ankle prostheses," *J. Biomech.*, Vol. 37, no. 10, 2004.

12. Hatze, H., "The fundamental problem of myoskeletal inverse dynamics and its implications," *J. Biomech.*, Vol. 35, no. 1, 2002.

13. Jiang, X., M. Gholami, M. Khoshnam, J. J. Eng, and C. Menon, "Estimation of ankle joint power during walking using two inertial sensors," *Sensors (Basel)*, Vol. 19, no. 12, 2019.

14. De Luca, C., *Electromyography.* John Wiley Sons, Inc., 2006.

15. Xiong, D., D. Zhang, X. Zhao, and Y. Zhao, "Deep Learning for EMG-based Human-Machine Interaction: A Review," *IEEE/CAA J. Autom. Sin.*, Vol. 8, no. 3, 2021.

16. Morbidoni, C., A. Cucchiarelli, S. Fioretti, and F. Di Nardo, "A deep learning approach to EMG-based classification of gait phases during level ground walking," *Electron.*, Vol. 8, no. 8, 2019.

17. Chen, J., X. Zhang, Y. Cheng, and N. Xi, "Surface EMG based continuous estimation of human lower limb joint angles by using deep belief networks," *Biomed. Signal Process. Control*, Vol. 40, 2018.

18. Ardestani, M. M., X. Zhang, L. Wang, Q. Lian, Y. Liu, J. He, D. Li, and Z. Jin, "Human lower extremity joint moment prediction: A wavelet neural network approach," *Expert Syst. Appl.*, Vol. 41, no. 9, 2014.

19. Abiodun, O. I., A. Jantan, A. E. Omolara, K. V. Dada, N. A. E. Mohamed, and H. Arshad, "State-of-the-art in Artificial Neural Network Applications: A survey," *Heliyon*, Vol. 4, no. 11, 2018.

20. Lipton, Z. C., J. Berkowitz, and C. Elkan, "A Critical Review of Recurrent Neural Networks for Sequence Learning arXiv : 1506 . 00019v2 [cs . LG] 29 Jun 2015," *Int. J. Comput. Vis.*, Vol. 106, no. March 2013, 2015.

21. Gers, F. A., N. N. Schraudolph, and J. Schmidhuber, "Learning precise timing with LSTM recurrent networks," *J. Mach. Learn. Res.*, Vol. 3, no. 1, 2003.

22. Tsoi, A. C., *Electromyography*, pp. 1–26. Springer Berlin Heidelberg, 1998.

23. Mahesh, B., "Machine Learning Algorithms-A Review Machine Learning Algorithms-A Review View project Self Flowing Generator View project Batta Mahesh Independent Researcher Machine Learning Algorithms-A Review," *Int. J. Sci. Res.*, 2018.

24. Zhang, L., Z. Li, Y. Hu, C. Smith, E. M. Farewik, and R. Wang, "Ankle Joint Torque Estimation Using an EMG-Driven Neuromusculoskeletal Model and an Artificial Neural Network Model," *IEEE Trans. Autom. Sci. Eng.*, Vol. 18, no. 2, 2021.

25. Dallali, H., L. Knop, L. Castelino, E. Ficanha, and M. Rastgaar, "Estimating the multivariable human ankle impedance in dorsi-plantarflexion and inversion-eversion directions using EMG signals and artificial neural networks," *Int. J. Intell. Robot. Appl.*, Vol. 1, no. 1, 2017.

26. Siu, H. C., J. Sloboda, R. J. McKindles, and L. A. Stirling, "Ankle torque estimation during locomotion from surface electromyography and accelerometry," in *Proc. IEEE RAS EMBS Int. Conf. Biomed. Robot. Biomechatronics*, Vol. 2020-Novem, 2020.

27. Zangene, A. R., A. Abbasi, and K. Nazarpour, "Estimation of lower limb kinematics during squat task in different loading using semg activity and deep recurrent neural networks," *Sensors*, Vol. 21, no. 23, 2021.

28. Seo, K., Y. J. Park, J. Lee, S. Hyung, M. Lee, J. Kim, H. Choi, and Y. Shim, "RNN-based on-line continuous gait phase estimation from shank-mounted imus to control ankle exoskeletons," in *IEEE Int. Conf. Rehabil. Robot.*, Vol. 2019-June, 2019.

29. Keles, A. D., and C. Yücesoy, "Development of artificial neural network based active ankle prosthesis algorithm using gait analysis data," in *2017 21st Natl. Biomed. Eng. Meet. BIYOMUT 2017*, 2018.

30. Keles, A. D., and C. A. Yucesoy, "Development of a neural network based control algorithm for powered ankle prosthesis," *J. Biomech.*, Vol. 113, 2020.

31. Lencioni, T., I. Carpinella, M. Rabuffetti, A. Marzegan, and M. Ferrarin, "Human kinematic, kinetic and EMG data during different walking and stair ascending and descending tasks," *Sci. Data*, Vol. 6, no. 1, 2019.

32. Paulsen, F., and J. Waschike, *Sobotta Atlas of Anatomy*, Vol. 65. Elsevier Health Sciences, 2018.

33. Valerie L Winslow, *Classic Human Anatomy in Motion: The Artist's Guide to the Dynamics of Figure Drawing.* Berkeley : Watson-Guptill Publications, 2015.

34. Pandy, M. G., and T. P. Andriacchi, "Muscle and joint function in human locomotion," 2010.

35. Eesa, A. S., and W. K. Arabo, "A Normalization Methods for Backpropagation: A Comparative Study," *Sci. J. Univ. Zakho*, Vol. 5, no. 4, 2017.

36. Patro, S. K., and K. K. Sahu, "Normalization: A Preprocessing Stage," *IARJSET*, 2015.

37. Márquez-Figueroa, S., Y. S. Shmaliy, and O. Ibarra-Manzano, "Analysis and Smoothing of EMG Signal Envelope Using Kalman and UFIR Filtering under Colored Measurement Noise," *MATEC Web Conf.*, Vol. 292, 2019.

38. Li, G., J. Li, Z. Ju, Y. Sun, and J. Kong, "A novel feature extraction method for machine learning based on surface electromyography from healthy brain," *Neural Comput. Appl.*, Vol. 31, no. 12, 2019.

39. Holm, S., and P. K. Eide, "The frequency domain versus time domain methods for processing of intracranial pressure (ICP) signals," *Med. Eng. Phys.*, Vol. 30, no. 2, 2008.

40. Asghari Oskoei, M., and H. Hu, "Myoelectric control systems-A survey," 2007.

41. Smith, S. W., *Digital Signal Processing: A Practical Guide for Engineers and Scientists*, Vol. 17. 2003.

42. Jang, G., J. Kim, Y. Choi, and J. Yim, "Human shoulder motion extraction using EMG signals," *Int. J. Precis. Eng. Manuf.*, Vol. 15, no. 10, 2014.

43. Yang, C., S. Chang, P. Liang, Z. Li, and C. Y. Su, "Teleoperated robot writing using EMG signals," in *2015 IEEE Int. Conf. Inf. Autom. ICIA 2015 - conjunction with 2015 IEEE Int. Conf. Autom. Logist.*, 2015.

44. Schmidt, R. M., "Recurrent Neural Networks (RNNs): A Gentle Introduction and Overview," *arXiv*, Vol. abs/1912.05911, no. 1, pp. 1–16, 2019.

45. MATLAB, "Deep Learning Toolbox Documentation." https://www.mathworks.com/help/deeplearning/index.html, 2013.

46. Mukaka, M. M., "Statistics corner: A guide to appropriate use of correlation coefficient in medical research," *Malawi Med. J.*, Vol. 24, no. 3, 2012.

47. Schober, P., and L. A. Schwarte, "Correlation coefficients: Appropriate use and interpretation," *Anesth. Analg.*, Vol. 126, no. 5, pp. 1763–1768, 2018.

48. Senanayake, D., S. Halgamuge, and D. C. Ackland, "Real-time conversion of inertial measurement unit data to ankle joint angles using deep neural networks," *J. Biomech.*, Vol. 125, 2021.

49. Hahn, M. E., and K. B. O'Keefe, "A neural network model for estimation of net joint moments during normal gait," *J. Musculoskelet. Res.*, Vol. 11, no. 3, 2008.

50. Zelik, K. E., and P. G. Adamczyk, "A unified perspective on ankle push-off in human walking," *J. Exp. Biol.*, Vol. 219, no. 23, 2016.